Optical generation of many-spin entangled states in a quantum well

R. Merlin[a], J. M. Bao[*a], A. V. Bragas[+a], J. K. Furdyna[b]
[a] FOCUS Center and Dept. of Physics, Univ. Michigan, Ann Arbor, MI, USA 48109-1120;
[b]Dept. of Physics, Univ. Notre Dame, IN USA 46556

ABSTRACT

A quantum-mechanical many-particle system may exhibit non-local behavior in that measurements performed on one of the particles can affect a second one that is far apart. These so-called entangled states are crucial for the implementation of quantum information protocols and gates for quantum computation. Here, we use ultrafast optical pulses and coherent techniques to create and control spin entangled states in an ensemble of up to three non-interacting electrons bound to donors in a CdTe quantum well. Our method, relying on the exchange interaction between localized excitons and paramagnetic impurities, can in principle be applied to entangle an arbitrarily large number of spins.

Keywords: quantum wells, quantum computation, entanglement, spin-flip transitions, ultrafast optics, Raman scattering

1. INTRODUCTION

The problem of quantum entanglement has attracted much attention since the early days of quantum mechanics. For pure states, entanglement refers to non-factorable wavefunctions that exhibit non-locality, i.e., correlations that violate Bellís inequalities.[1] As exemplified by the famous Einstein-Podolsky-Rosen paradox, one of the most intriguing features of quantum behavior is that non-interacting parts of a system can show non-local correlations reflecting interactions that occurred in the past. In this respect, entangled states of *macroscopic* systems - the so-called Schrˆdinger cats - are of particular interest because their properties defy classical intuition. While the quantum/classical boundary has been discussed in the theoretical literature for more than 50 years,[1] it is only in the past decade that careful experiments that probe this boundary have been carried out.[2] It is also recently that specific models have been solved to reveal the mechanisms by which coupling to the environment restores classical reality through decoherence.[2]

Following the proposal by Deutsch for a quantum computer in 1985, the building of a quantum cryptography machine by Bennett et al. in 1989,[2] and the discoveries (by Shor[3] in 1994 and by Grover[4] in 1996) of quantum algorithms that outperform those of classical computation, research on the foundations of quantum mechanics has now moved to the center of the new field of quantum information.[2] As a result, the questions of entanglement and decoherence have acquired practical significance. The generation of a multiple-qubit entangled state is an important step for quantum computing. Particularly important for information processing are those operations associated with gate sets that can perform any quantum computation, such as the combination of single-qubit operations with the 2-qubit controlled-NOT (C-NOT) gate which relies on entanglement.[2] Although techniques to entangle two particles and, in particular, two photons have been known for some time,[5] it is only recently that many (up to four)-particle entanglement has been demonstrated experimentally.[6,7] The various schemes that have been proposed for the implementation of a quantum computer use different strategies for attaining entangled states. These methods can be categorized into two classes according to whether or not the entanglement between qubits is mediated by an auxiliary particle. In schemes based on nuclear magnetic resonance (NMR)[2]and for excitons in quantum dots, the source of entanglement is the direct spin-spin exchange or Coulomb interactions which cannot be controlled experimentally.[8] An example belonging to the second class is the ion trap system where center-of-mass phonons induce interactions between two non-interacting ions.[7] Our entanglement scheme in which an exciton is created optically to mediate interactions between non-interacting electrons in a quantum well belongs to the second category.[9,10]

[*] Present address: Division of Engineering and Applied Sciences, Harvard University, Cambridge, MA 02138, USA
[+] Present address: FCEyN, Univ. Buenos Aires, Ciudad Universitaria, 1428 Buenos Aires Argentina

Noise and Information in Nanoelectronics, Sensors, and Standards II, edited by Janusz M. Smulko, Yaroslav Blanter, Mark I. Dykman, Laszlo B. Kish, Proc. of SPIE Vol. 5472 (SPIE, Bellingham, WA, 2004) · 0277-786X/04/$15 · doi: 10.1117/12.548108

Many systems have been proposed as candidates for the implementation of a quantum computer, and basic quantum operations have been already demonstrated. Methods associated with NMR, trapped ions and cavity quantum electrodynamics are just a few examples.[11-13] In addition, solid-state approaches to quantum computing have been implemented using electrons states in quantum dots or the spins of impurities in a semiconductor.[14,15] The advantage of solid state devices is the fact that they can be integrated and scaled using modern fabrication techniques. In our experiments, the qubits are embodied by the spins of electrons bound to donors in a $Cd_{1-x}Mn_xTe$/MnTe quantum well.

$Cd_{1-x}Mn_xTe$ is a dilute magnetic semiconductor (DMS). These are alloys for which many physical properties such as the lattice parameters and the bandgap can be widely tuned by varying the concentration of a paramagnetic ion.[16,17] This tunability makes $Cd_{1-x}Mn_xTe$ a very useful system for bandgap engineering and device applications. Depending on the manganese concentration and temperature, $Cd_{1-x}Mn_xTe$ exhibits paramagnetic, antiferromagnetic or spin-glass phases.[16,17] Many of the unique properties of DMS materials stem from the so-called *sp-d* exchange interaction between band electrons and localized magnetic ions. This interaction leads to unusually large Zeeman splittings and a giant Faraday rotation.[16,17] Because of *sp-d* exchange, the *g*yromagnetic *g*-factors can be amplified by as much as two orders of magnitude and, as a result, the effective magnetic field acting on carriers can be significantly larger than the external field. This greatly reduces the need for a strong magnetic source in certain applications. As mentioned above, our qubits are associated with donor impurities. Donors not introduced intentionally (e.g., indium) have been identified in various works with concentration ranging from 10^{14} to 10^{16} per cm^3.[16,17] Since the wave function of a donor-bound electron extends over many lattice sites, donor-bound and free electrons have a similar exchange interaction with magnetic ions, so that their *g*-factors are approximately the same. Two other properties of $Cd_{1-x}Mn_xTe$ are crucial to our spin entanglement method. First, due to quantum confinement and spin-orbit coupling, the spin of the heavy hole is oriented along the sample growth direction, the *z*-axis, independent of the direction of the external magnetic field (this property is shared by all zinc-blend semiconductors).[20,21] Second, the exchange interaction between the donor electrons and the photoexcited heavy-hole of the exciton provides the effective interaction between the otherwise non-interacting electrons.[22,23]

The outline of this work is as follows. We will first present a brief introduction to impulsive stimulated Raman scattering and a model for multi-spin entanglement in Section 2, experimental observations and discussions will be given in Section 3.

2. MODEL FOR THE GENERATION OF MULTI-SPIN ENTANGLEMENT

2.1 Stimulated Raman scattering and coherent superpositions

Coherences between quantum states can be established using ultrafast laser pulses through impulsive stimulated Raman scattering (ISRS).[24-26] Because of its relevance to our method for spin entanglement, we discuss briefly in the following ISRS for atomic-like systems (we note that the generation of coherent phonons using ISRS, as discussed in Ref. [27] can be easily modified to account for other extended modes, such as intersubband density oscillations and plasmons.) The relevant Hamiltonian is:

$$H = H_0 + V(t) \tag{1}$$

where the spectrum of H_0 is shown in Fig. 1. Here

$$H_0 \mid i >= E_i \mid i > \tag{2}$$

for i = 1,2 and $i = l, l+1,..$ E_i is the eigenenergy associated with the ith level. The light-medium interaction is given as:

$$V(t) = -d \bullet E(t), \tag{3}$$

where d is the electric-dipole operator and $E(t)$ is a time dependent electric field (to simplify the notation, d and E are treated as scalars). States |1> and |2> are low-lying states associated with magnetic, electronic or vibrational degrees of freedom whereas the set |*l*> represents high-lying electronically excited states (in our experiments, the energies of |*l*> are close to those of the band gap). We assume that dipole transitions between both |1> and |2>, and the excited states |*l*> are allowed, i.e.,

$$d_{l2} = < l \mid d \mid 2 > \neq 0\,,\ d_{l1} = < l \mid d \mid 1 > \neq 0\,, \qquad (4)$$

and also that the system is initially in the ground state |1>

We now use the Hamiltonian of Eq. (1) to illustrate the concept of ISRS. Specifically, we want to explain the relationship between time-resolved data and the induced Raman coherences (in spontaneous Raman scattering (Stokes), an incident photon induces a transition from the ground state |1> to an intermediate state |*l*>, and a Stokes photon is emitted when the state |*l*> relaxes to the final excited state |2>). A time-resolved pump-probe experiment is conveniently divided into two steps. First, a pump pulse generates a coherent superposition state and, then, a weaker time-delayed probe pulse is used to measure the changes in the optical constants induced by the Raman coherence. Let us first look at how the pump pulse establishes a coherence between states |1> and |2>. If the initial wave function is the ground state |1>, the time dependent wave function after the system interacts with the pump pulse can be written as:

$$| \Psi(t) > = e^{-i\omega_1 t} \mid 1 > + C_2 e^{-i\omega_2 t} \mid 2 > + \sum_l C_l e^{-i\omega_l t} \mid l >\,, \qquad (5)$$

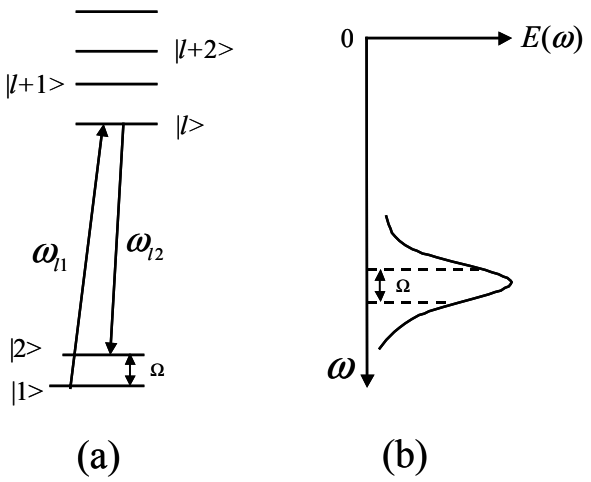

Fig. 1. (a) Excitation of a Raman transition |1> → |2> involving an electronically excited state |*l*>. (b) For ultrafast laser pulses of central frequency ω_C, the coherence between state |1> and |2> is driven by two fields with frequencies contained within the pulse spectrum.

where $\omega_i = E_i / \hbar$. C_2 and C_l are time-dependent coefficients with $|C_2| << 1$ and $|C_l| << 1$ so that the ground state population does not vary much. A standard second-order perturbation calculation gives:

$$C_2(t=\infty) = -\sum_l \hbar^2 \frac{d_{2l} d_{l1}}{2\pi} \int \frac{E(\omega) E^*(\omega - \Omega)}{-i\omega + i\omega_l - i\omega_1} d\omega\,, \qquad (6)$$

where $E(\omega) = \int E(t) e^{i\omega t} dt$ is the Fourier transform of the electric field. We see from this expression that the following factors determine C_2. First, the matrix elements d_{2l} and d_{l1} must be nonzero. Second, the bandwidth of the pump pulse must be greater than the energy separation $\hbar\Omega$. In other words, the pulse must have a large frequency overlap between $E(\omega)$ and $E(\omega - \Omega)$ to generate a significant amplitude. The coherence is driven by infinite pairs of fields $E(\omega)$ and $E(\omega\text{-}\Omega)$ contained in the pulse band spectrum.

The levels |1> and |2> are usually vibrational levels or magnetic Zeeman-split states which have a much longer coherence time than that of the coherence between |1> (or |2>) and level |*l*>. In the *non-resonant* case, for which the central energy of the laser pulse is $\omega_c << \omega_l$, the excited state populations are negligible, i. e., $C_l \equiv 0$. Hence, after a certain time-delay τ, when the probe pulse interacts with the medium, the wave function is

$$| \Psi > = e^{-i\omega_1 \tau} \mid 1 > + C_2 e^{-i\omega_2 \tau} \mid 2 > \qquad (7)$$

To probe this coherent superposition, we use a nonlinear process. The corresponding nonlinear susceptibility χ^{NL} can be calculated by considering the interaction between a monochromatic electric field with the system. Using perturbation theory we get to lowest order

$$\chi^{NL}_{\omega}(t) = \sum_l \frac{C_2^* d_{2l} d_{l1} e^{i\Omega\tau} e^{i\Omega t}}{\hbar(\omega - \omega_{l1})} + \sum_l \frac{C_2 d_{1l} d_{l2} e^{-i\Omega\tau} e^{-i\Omega t}}{\hbar(\omega - \omega_{l2})} = A(\omega) e^{i\Omega\tau} e^{i\Omega t} + A^*(\omega) e^{-i\Omega\tau} e^{-i\Omega t}\,, \qquad (8)$$

where $A(\omega) = \sum_l C_2^* d_{2l} d_{l1} \hbar^{-1} (\omega - \omega_{l1})^{-1}$. Eq. (8) shows that Stokes and anti-Stokes polarizations are created due to the induced Raman coherence.

The experiments are usually performed in the reflection geometry with nearly normal incidence. Hence, we have that

$$E_{\text{ref}} = \frac{n-1}{n+1} E_{\text{in}} \tag{9}$$

where

$$n = \sqrt{1+4\pi(\chi_0 + \chi^{\text{NL}})}\,. \tag{10}$$

E_{in} (E_{ref}) is the incident (reflected) electrical field, n is the refractive index of the medium and χ_0 is the linear susceptibility. Expanding Eq. (9) and (10) in powers of χ^{NL} to lowest order , we have

$$\frac{n-1}{n+1} \approx \frac{n_0-1}{n_0+1} + \frac{4\pi}{n_0(n_0+1)^2}\chi^{\text{NL}}, \tag{11}$$

where $n_0 = \sqrt{1+4\pi\chi_0}$ is the refractive index in the absence of the coherence. Let $E_{\text{in}}(t) = \int E_{\text{in}}(\omega)e^{-i\omega t}dt$. Substituting Eq. (11) and (8) into Eq. (9), we obtain the reflected field

$$E_{\text{ref}}(\omega) = \alpha(\omega)E_{\text{in}}(\omega) + \beta(\omega)A(\omega)e^{i\Omega\tau}E_{\text{in}}(\omega-\Omega) + \beta(\omega)A^*(\omega)e^{-i\Omega\tau}E_{\text{in}}(\omega+\Omega)\,. \tag{12}$$

where $\alpha(\omega) = (n_0-1)/(n_0+1)$ and $\beta(\omega) = 4\pi/n_0(n_0+1)^2$. Thus, the change in intensity at frequency ω due to the induced coherence is:

$$\Delta R(\omega) = |E_{\text{ref}}(\omega)|^2 - |\alpha(\omega)E_{\text{in}}(\omega)|^2 = \\ \text{Re}\{\alpha(\omega)\beta^*(\omega)A^*(\omega)E_{\text{in}}(\omega)E_{\text{in}}^*(\omega-\Omega)e^{-i\Omega\tau} + \alpha(\omega)\beta^*(\omega)A(\omega)E_{\text{in}}(\omega)E_{\text{in}}^*(\omega+\Omega)e^{i\Omega\tau}\} \tag{13}$$

where the second-order term has been dropped. This expression can be rewritten as:

$$\Delta R(\omega) = \gamma(\omega)\sin(\Omega\tau+\phi)\,, \tag{14}$$

where $\gamma(\omega)$ and ϕ are constants. The total change in the intensity of the reflected probe is obtained by integrating over the whole spectrum:

$$\Delta R = \int \Delta R(\omega)d\omega = \sin(\Omega\tau+\phi)\int \gamma(\omega)d\omega\,. \tag{15}$$

Eq. (15) indicates that the reflectivity of the probe pulse oscillates with frequency Ω as a function of the time delay τ between the pump and probe pulses. Further, Eq. (14) shows that the spectral intensity of the reflected probe experiences the same oscillatory behavior. Eq. (13) shows that the differential reflectivity depends on the overlap between $E_{\text{in}}(\omega)$ and $E_{\text{in}}(\omega-\Omega)$. This result is similar to Eq. (6), where the induced coherence depends on the bandwidth of the pump pulse. Combining both pump and probe processes, we get

$$\Delta R \propto I_{\text{pu}} I_{\text{pr}}\,. \tag{16}$$

This equation indicates that the overall signal is proportional to the product of the pump and probe intensities. This property allows us to detect the signal with lock-in techniques by simply chopping either the pump beam or both beams.

In the above description, we only considered the coherence between the two lowest-lying levels. In the case of multiple coherences, the total signal is a linear superposition of terms such as those in Eq. (15). With Fourier transform and other spectral analysis techniques, we can retrieve the spectral information about multiple coherences.

The above analysis applies to transparent materials. For resonant excitation and, in particular, when the pulse width is greater than the energy separation between high-lying excited states $|k\rangle$ ($k = l, l+1,\ldots$), the pump pulse may also induce coherences between these states. In the physical-chemistry literature, these are called excited-state coherences whereas the coherence between the state $|1\rangle$ and $|2\rangle$ is referred to as a ground-state coherence.[28,29] Like ground-state coherences, excited-state coherences will also modify the spectrum and intensity of the reflected probe beam, and these changes can also be measured in pump-probe experiments.

Finally, we note that the selection rules for spontaneous and impulsive stimulated Raman scattering are the same although the tensors that apply to the generation and detection are considerably different for opaque media.[30,31] The selection rules are crucial to determine as to whether or not the generation mechanism for coherent superposition states is stimulated Raman scattering.

2.2 Multi-spin coherence: donors and Mn^{2+} spins in $Cd_{1-x}Mn_xTe$

Generally, an existing interaction or, for non-interacting systems, an interaction that existed in the past is required to create an entangled state. In our case, an optically excited exciton provides the interaction between N electrons bound to donors. The Hamiltonian pertinent to our problem is

$$H = H_0 + V(t) = [\,|g\rangle H_g \langle g|\,] + [\,|e\rangle H_e \langle e|\,] + V(t) \tag{17}$$

where $|g\rangle$ is the ground state of the solid and $|e\rangle$ is the lowest state of an exciton with energy E_e.[20,32] The Hamiltonian $V(t) = -d \cdot E(t)$ accounts for the interaction of the exciton with the light pulses. H_g describes the interaction of donor-bound electrons with the external magnetic field. It is given by

$$H_g = \sum_{i=1}^{N} g\mu_B \mathbf{s}_i \cdot \mathbf{B} \;=\; g\mu_B \mathbf{S} \cdot \mathbf{B}\,, \tag{18}$$

where $\mathbf{s}_i$ is the spin of the ith electron, $\mathbf{S} = \sum_{i=1,..,N} \mathbf{s}_i$ is the total spin of N electrons, $\mathbf{B}$ is the applied magnetic field and g is gyromagnetic factor. The Hamiltonian H_e is given by

$$H_e = E_e + g\mu_B \mathbf{S} \cdot \mathbf{B} - \kappa \mathbf{S} \cdot \mathbf{J} = E_e + g\mu_B \mathbf{S} \cdot \mathbf{B}_w\,, \tag{19}$$

where $\mathbf{J}$ is the spin of heavy hole of the exciton, $|\mathbf{J}|=3/2$, $\mathbf{B}_w = \mathbf{B} - \kappa\mathbf{J}/g\mu_B$ is the effective magnetic field, E_e is the energy of the exciton and κ is the coupling constant associated with the exchange interaction between electrons and heavy holes, which depends on the overlap between their wave functions.[22,23] We assume that each bound electron experiences the same exchange interaction with the excitonís heavy-hole. Because of spin-orbit coupling and quantum confinement, and provided the external magnetic field is not too strong, the heavy-hole spin is oriented along the sample growth direction.[21,33] Our experiments were performed in the Voigt configuration such that the applied magnetic field is parallel to the well surface in the x direction.

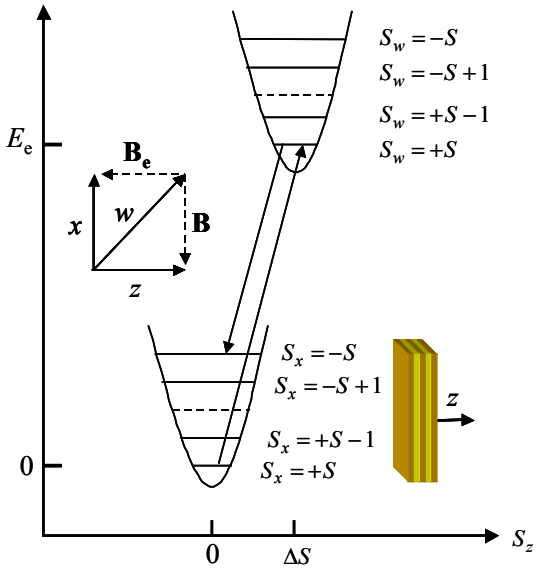

Fig. 2. Generic level structure of a quantum-well system of donor-bound electrons coupled to a localized exciton of energy E_e. Optical transitions are depicted by arrows. $\mathbf{B}$ is the external magnetic field and $\mathbf{B}_e$ is an effective field describing the interaction between the donor electrons and the exciton heavy-hole. The energy diagram is not to scale, E_e is much greater than Zeeman-split energy. Parabolas represent the vibrational analog for $S >> 1$.

The unperturbed Hamiltonian can be solved exactly. The eigenfunctions are separable into products of bound-electron spin and exciton wave functions. The energy levels are shown schematically in Fig. 2. The levels at the bottom of the figure are of the form $|S-k\rangle_x \otimes |g\rangle$, where $|S-k\rangle_x$ is one of the Zeeman-split states of the total spin $\mathbf{S}$, quantized along the x direction. Here, $\mathbf{S}^2 |S-k\rangle_x = S(S+1)|S-k\rangle_x$ and $S=N/2$. Also, $H_0 |S-k\rangle_x \otimes |g\rangle = k\hbar\Omega_0 |S-k\rangle_x \otimes |g\rangle$ with $0 \le k \le 2S$; $\Omega_0 = g\mu_B B/\hbar$ is the single electron Zeeman splitting frequency. In the presence of the exciton, $H_0 |S-l\rangle_w \otimes |e\rangle = (E_e + l\hbar\Omega) |S-l\rangle_w \otimes |e\rangle$ where $|S-l\rangle_w$ is the Zeeman-split spin state for which the quantization axis is parallel to $\mathbf{B}_w$ and $\Omega = g\mu_B B_w/\hbar$. We note that, since the heavy-hole spin $\mathbf{J}$ is along the z-direction, $\mathbf{B}_w$ and $\mathbf{B}$ are in different directions. This property is crucial to the implementation of our method. Because Zeeman states along different quantization axes are not orthogonal to each other, a coherence between $|S-k\rangle_x \otimes |g\rangle$ and $|S-l\rangle_w \otimes |e\rangle$ can be established by means of a single electric dipole transition. In addition, a Raman coherence between

$|S-k\rangle_x \otimes |g>$ and $|S-m\rangle_x \otimes |g>$ can be generated by using two dipole transitions and $|S-l\rangle_w \otimes |e>$ as the intermediate. A Raman coherence between these states can be established by two laser fields separated in energy by $(m-k)\hbar\Omega_0$. As an example, consider the so-called maximally entangled Bell State $\psi_{\text{Bell}} = (|-S>_x + |S>_x)/\sqrt{2}$ which is a superposition of the ground state $|S>_x$ and the highest excited state $|-S>_x$.[1] This state can be generated by establishing a Raman coherence from state $|S\rangle$ to $|-S\rangle$, through an intermediate state $|S\rangle_w$ as depicted by the two arrows in Fig. 2. A properly tailored optical pulse can in principle generate a predefined superposition of the 2S+1 states $|S-k\rangle_x$ of the form

$$\psi(t) = \sum_{k=0}^{2S} C_k e^{-ik\Omega_0 t} |S-k\rangle_x \tag{20}$$

The constants C_k can, in principle, be controlled experimentally.

Our model can be understood from a different point of view. In the case where the total spin $S >> 1$, the spin can be mapped into the dynamics of a simple harmonic oscillator.[37] After some algebra, we get

$$H_e = E_e - g\mu_B B(S+\frac{1}{2}) - \frac{S\kappa^2 J_z^2}{2\mu_B gB} + \frac{g\mu_B B}{2S}(\mathbf{S}_z - \frac{S\kappa J_z}{\mu_B gB})^2 + \frac{g\mu_B B}{2S}\mathbf{S}_y^2 . \tag{21}$$

Since $[\mathbf{S}_z, \mathbf{S}_y] = i\hbar\mathbf{S}_x \approx i\hbar S$, the transformed Hamiltonian is a simple harmonic oscillator with potential given by $U(\mathbf{S}_z) = (\mu_B gB/2S)[\mathbf{S}_z - S\kappa J_z/\mu_B gB]^2$. This represents a parabola which is displaced by $\Delta S_z = S\kappa J_z/\mu_B gB$ from the parabola associated with H_g which can be easily obtained by letting $\kappa = 0$. The two parabolas are shown in Fig. 2. Using this transformation, the equally spaced Zeeman states are mapped onto equally separated harmonic eigenstates. The spin-flip problem is then transformed to that of molecular vibrations coupled to two, ground and excited, electronic states. The coupling is determined by the displacement of the two parabolas. The later problem has been extensively studied and it is well understood. There is a large literature on coherent control of molecular vibrations using laser fields, which translates into coherent spin control in our problem. The available techniques include pulse shaping, four-wave-mixing, stimulated Raman adiabatic passage (STIRAP) and pump-dump.[34-36,38] In this sense, an arbitrary spin entangled state can be generated by a properly shaped pulse. Based on our early discussion, an entangled state of the form given in Eq. (20) is expected to modulate the optical properties of the sample at frequencies which are multiples of Ω_o. As shown below, the fundamental and its harmonics can be observed by measuring the differential reflectivity in a time-domain pump-probe experiment. In the case of a product state of N independent electrons, only Ω_o will be observed. Because an electron has spin $s = \Omega$, the observation of the Nth harmonic indicates that an entanglement of N electrons has been achieved.

3. EXPERIMENTS

3.1 Sample characterization: photoluminescence and (spontaneous) Raman scattering measurements

Our sample is a CdTe/MnTe superlattice consisting of 100 periods of 58 ≈ CdTe wells with 19≈ MnTe barriers. It was grown by Molecular Beam Epitaxy (MBE) on a [001] CdTe substrate. The properties of $Cd_{1-x}Mn_xTe$ are fairly well understood.[16,17] Bulk CdTe is a non-magnetic semiconductor with a bandgap of 1.6eV. The bandgap of MnTe is 3.23 eV. Due to the diffusion of Mn^{2+} ions into the CdTe well from the interface, the originally non-magnetic CdTe transforms into a $Cd_{1-x}Mn_xTe$ DMS quantum well, with some average concentration x.

We used a 488.0 nm Ar^+-ion laser to measure the photoluminescence (PL) spectrum. A continuous wave (cw) tunable Ti-sapphire was used to perform PL excitation studies and spin-flip Raman scattering. The experiments were carried out using a superconducting optical cryostat, which provides magnetic fields up to 7 T. Pump-probe data were obtained under the same conditions as in the light scattering experiments, except that we used a tunable mode-locked Ti-sapphire laser (Spectra-Physics Tsunami). The central wavelength of the pulses can be tuned around the bandgap of the quantum wells from 720nm to 776nm.

PL measurements are widely used to determine the energy of excitons near the band gap. Fig. 3 shows the PL spectrum of the sample. The polarizations of the incident and scattered light were not analyzed. Features below 1.70eV are associated with transitions involving heavy-hole state. Note that quantum confinement not only increases the band gap of the quantum well, but it also lifts the degeneracy between heavy and light hole bands. Given that the bandgap of bulk CdTe is 1.60 eV, the observed blue shift of about 80 meV for the gap is a manifestation of quantum confinement. The fact that the position of the PL is red-shifted (by ~ 6meV at $B = 0$) with respect to the maximum of the PLE spectrum (not shown) indicates that the PL is associated with the recombination of localized excitons.[20] Localized excitons have been identified in similar quantum well DMS systems as the dominant intermediate states in resonant spin-flip Raman scattering.[20] The exact source of exciton localization is not well understood. However, it is believed that interface roughness or the interaction with impurities contribute to the localization. Because excitons at different sites have different excitation energy, the PL line is inhomogeneously broadened (the half width is ~ 30 cm^{-1}). In our time-domain experiments, the laser is tuned near the heavy-hole exciton, and the laser bandwidth is much narrower than the separation between the heavy-hole and the light-hole state (at ~ 1.73 ev), so that the later states will not be considered in the following.

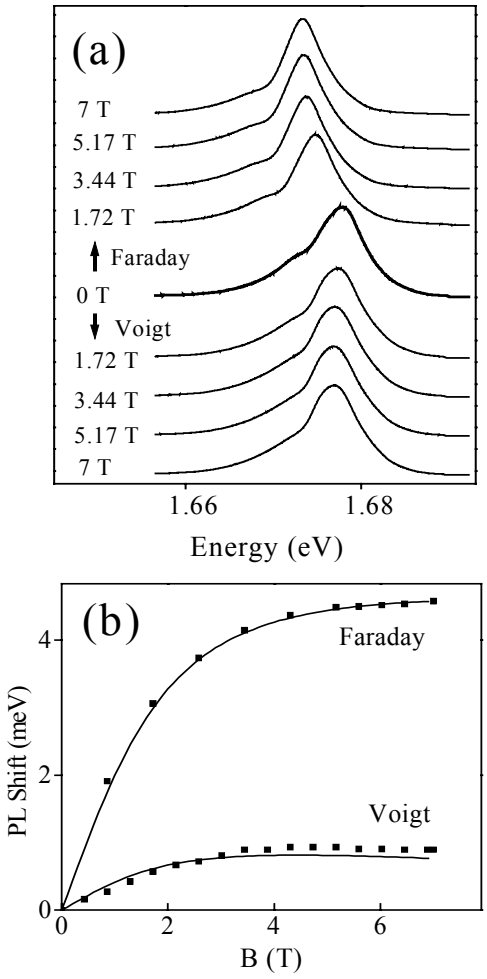

Fig. 3. (a) PL at various magnetic fields in the Faraday and Voigt configurations. The zero-field PL is also shown. (b) PL shifts versus magnetic field. The data in the Voigt configuration is fitted with x = 0.41%, T = 3.5K, while fitting parameters for the Faraday configuration are x = 0.36%, T = 3.5K.

Excitons in $Cd_{1-x}Mn_xTe$ interact strongly with the spins of localized manganese ions through the *sp-d* exchange interaction leading primarily to a strong dependence of the band edge on magnetic field and manganese concentration.[16,17] This dependence can be used to determine the average manganese concentration x of our sample. Under an applied magnetic field, both the electron and the heavy hole experience large Zeeman splittings in the Faraday and Voigt configurations.[16,17] The exciton Zeeman splitting depends on the manganese concentration and temperature. For the electron, the Zeeman term can be written as:[16,17]

$$E_{\pm} = \pm(g_c \mu_B H - N_0 \alpha x < S_z >)/2\,, \qquad (22)$$

where E_+ (E_-) is the energy of the electron with spin up (down). The Landau level dependence has been omitted for simplicity. Here $g_c \approx -1.6$ is the intrinsic gyromagnetic factor of the electron in CdTe, $N_0\alpha \approx$ 220meV characterizes the exchange interaction between the electron and the ions, x is the concentration of Mn^{2+} ion in the CdTe well, and $<S_z>$ is the average spin of a single Mn^{2+} ion, given by $-(5/2)B_{5/2}(\mu_B g H / k_B T)$, where $B_{5/2}$ is the Brillouin function. For the heavy-hole in the Faraday configuration, the Zeeman splittings are given by a similar expression, except that the intrinsic gyromagnetic factor is $g_h \approx 0.65$[39] and the exchange interaction is $N_0\beta \approx$ -880meV. In the Voigt configuration, the heavy hole exhibits no Zeeman splitting at small fields since its spin is aligned along the z direction.

Due to the large Zeeman coupling, the PL peaks shift substantially to lower energy with increasing magnetic field. The PL shift in the Faraday configuration can be best fitted with x = 0.0036, while the curve in the Voigt configuration is the fit with x = 0.0041; both with T = 3.5 K. The obtained temperature from the fit is slightly higher than the temperature at which the experiment was performed, a fact that can be accounted for by laser heating. This difference is also observed in the pump-probe data. There are two factors which may contribute to the difference in the obtained manganese

concentrations. First, there are large errors in the determination of the PL since the peaks have a relatively large width and, second, there is considerable uncertainty as to the actual value of g_h. The value $g_h \approx 0.65$ is obtained by interpolation from measurements on a CdTe/$Cd_{0.85}Mg_{0.15}Te$ single quantum well.[39] The fact that g depends strongly on the well width is not important for our results. As it will be shown later, the spin-flip frequencies from spontaneous Raman and pump-probe agree with each other and both of them can be fitted with the same parameter $x = 0.0041$.

Light scattering is an important method for studying magnetic excitations. Using tunable cw lasers and resonant enhancement, weak excitations can be easily probed by Raman scattering. Relevant to our work are the observations of single donor spin-flip and up to three donor spin-flip transitions in CdS and ZnTe reported many years ago.[40-42] The multiple spin-flip scattering is enhanced when the laser energy is tuned to resonate with excitons at the bandgap. Spin-flip Raman scattering of donor-bound electrons in $Cd_{1-x}Mn_xTe$ and $Cd_{1-x}Mn_xTe$ quantum wells has been extensively studied.[18,19] Raman scattering by donor levels is usually performed at low incident power densities to avoid photo-excitation of free electrons. Since the g-factors for bound and free electrons are nearly the same, spin-flip frequencies for bound and free electrons are hard to distinguish except for their different power dependences since the intensity of donor Raman scattering is proportional to the laser power while that of photo-excited electrons increases as the square of the power.

Fig. 4 shows spin-flip transitions in the Voigt configuration. The inset shows the magnetic field dependence of the spin-flip frequency which is well described by Eq. (22). The PL shift in the Voigt configuration is also shown in the inset. The fact that the donor spin-flip frequency is almost twice as large as the PL shift can be easily understood since the spin-flip frequency involves transitions between spin up and down states while only the spin down state contributes to the PL shift in the Voigt configuration. The half width of the donor spin-flip is ~ 3 cm^{-1} which we attribute to inhomogeneous broadening since the spin-flip frequency is very sensitive to fluctuations in the local Mn^{2+} concentration.

Raman excitation of the donor spin-flip is a resonant effect. In our experiment, donor transitions can only be observed when the laser energy is tuned to resonate with the PL peak. A stronger spin-flip signal and its harmonics for donors

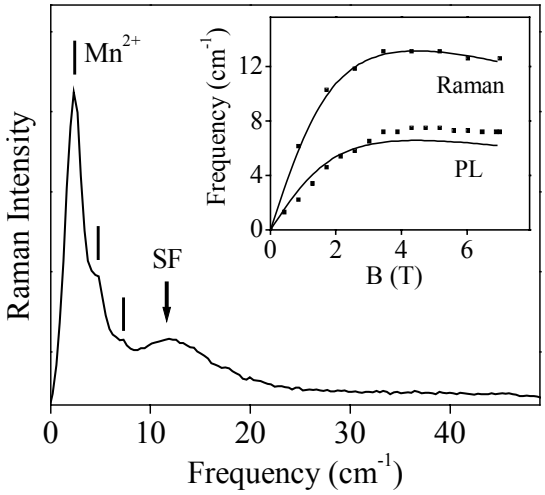

Fig. 4. Resonant Raman spectrum in the Voigt configuration for B = 2.6T and T=3.5K. The laser energy is 1.66eV. Bars indicate Mn^{2+} spin-flip harmonics. The peak labeled SF at 12 cm^{-1} is the donor spin-flip. The magnetic field dependence of SF is shown in the inset together with the PL shift in the Voigt configuration. Both curves are fits with x = 0.41% and T = 3.5K.

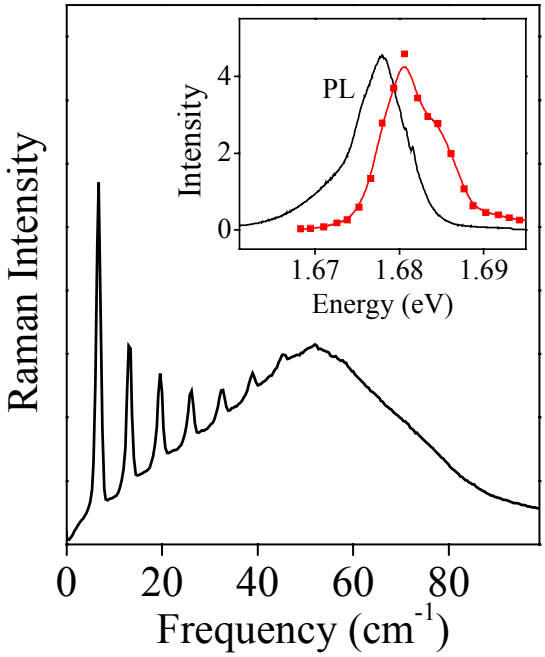

Fig. 5. Resonant multiple spin-flip of Mn^{2+} ions. The laser energy is 1.685eV, the broad feature is the PL. Inset: (red squares) Resonant Raman excitation spectrum of the first Mn^{2+} spin-flip.

should be expected from our model. However, when the laser is tuned closer to the PL maximum, the Mn^{2+} paramagnetic resonance (PR) and its harmonics become so strong that the donor spin-flip is very difficult to observe. In Fig. 4, we observe the first two harmonics of the PR line. Fig. 5 shows very strong multiple PR of Mn^{2+} ion when the laser is in resonance with localized excitons.[20] The tenth harmonic can be seen, which indicates that at least two Mn^{2+} ions are involved since the spin of Mn^{2+} is 5/2. In the inset of Fig. 5, we plot the Raman intensity of the PR line versus laser excitation energy (resonant Raman scattering). The fact that the resonant RS peak nearly coincides with the PL maximum indicates that localized excitons are the relevant intermediate states in Raman scattering.[20] The strongest Raman peak is observed when the laser is tuned to the outgoing resonance with localized excitons. The reason why we observed both donor and Mn^{2+} spin-flip is that we have donors as well as isolated Mn^{2+} in the well. Both donor electrons and Mn^{2+} interact with heavy holes, and our model applies to both of them. The *sp-d* exchange interaction between the heavy holes and Mn^{2+} ions in DMS is well understood. In bulk materials, but less so in quantum-well structures, extensive information on the exchange interaction between donor electrons and holes exists in the literature.[22,23,43-45] Note that the gyromagnetic factor for Mn^{2+} is about $g_{Mn} \approx 2$. Thus, signals from donors can be easily distinguished from that of Mn^{2+}.

3.2 Ultrafast time-domain experiments

Raman scattering measures the spin-flip frequency directly in the frequency domain, while ultrafast pump-probe experiments measure coherent oscillations in the time domain. The experiments were performed in the Voigt configuration, i. e., the external magnetic field is in the plane of the quantum-well.[46,47] We used circularly polarized pump pulses to excite a single spin component of the heavy hole so that the effective magnetic field $\kappa J_z \neq 0$.

The time-domain oscillations shown in Fig. 6 are for pump-probe experiments performed with the laser tuned below the quantum-well bandgap. The upper trace was obtained for a pulse central energy of 1.6 eV. In the bottom trace at 1.655 eV, the donor spin-flip transition is observed. The time-domain oscillations were analyzed using linear prediction (LP) methods which are widely used in NMR and other time-domain techniques to identify weak oscillations.[48] The parameters from the LP fit are used to generate the Fourier transform spectra. The LP results are shown in the insets of Fig. 6 as Fourier transform spectra. The top trace shows a single oscillation at 5.26cm^{-1} with B = 7 T. The frequency is linear with the magnetic field (not shown) with g = 1.6 which agrees extremely well with the electron g-factor in CdTe. Its amplitude is also linear with the pump power. According to these observations, the oscillations are assigned to coherent spin-flip transitions of electrons in the CdTe substrate. The bottom trace shows a different behavior. For the first 20ps, the signal is dominated by a high-frequency oscillation which decays after 20ps, and it is followed by a long lived, slow decaying oscillation. The frequency domain inset shows two peaks besides the electron spin-flip from the CdTe substrate. The sharp feature at ≈ 6.5 cm^{-1}, is the long-lived oscillation due to the Mn^{2+} ion PR. The oscillation frequency is linear with the magnetic field, and the obtained g-factor agrees well with Mn^{2+} spin-flip Raman scattering. The broad feature at about 9 cm^{-1}, which is the dominant oscillation in the first 20 ps, is due to the donor spin-flip. The dependence of its frequency on the magnetic field is the same as in the donor Raman spin-flip in

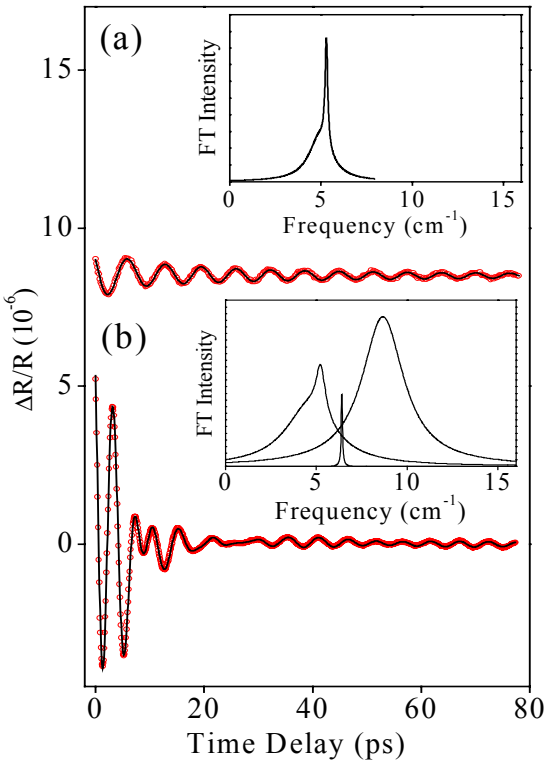

Fig. 6. Pump-probe differential reflectivity data at (a) $\hbar\omega_C$ = 1.60eV (below gap) and (b) $\hbar\omega_C$ =1.66eV (near resonance with localized excitons). Data are obtained at B = 7 T, T = 5 K. Curves are fits using the linear prediction method. The mode parameters gained from the fits were used to generate the associated Fourier transform spectra depicted in the insets. The main feature in (a) is due to spin-flip of bulk CdTe electrons. In (b), the sharp feature is due to Mn^{2+} paramagnetic resonance. The dominant feature at 9 cm^{-1} is associated with the spin-flip of donor electrons in the QW.

Fig. 4. Since the experiment is performed at 5K, the observed frequency is slightly lower than that from spontaneous Raman scattering.

As we tune the laser closer to the bandgap of the quantum well, the electron spin-flip signal from the substrate disappears. Typical pump-probe traces in resonance with localized excitons are shown in Figs. 7 and 8 for $\hbar\omega_C = 1.682$eV. The insets show the Fourier transform spectra. The spectra reveal several new oscillations at frequencies which are higher than those for laser energies below the gap. To identify the new features, we performed pump-probe experiments at different magnetic fields, the results of which are shown in Fig. 7(b). The various peaks are

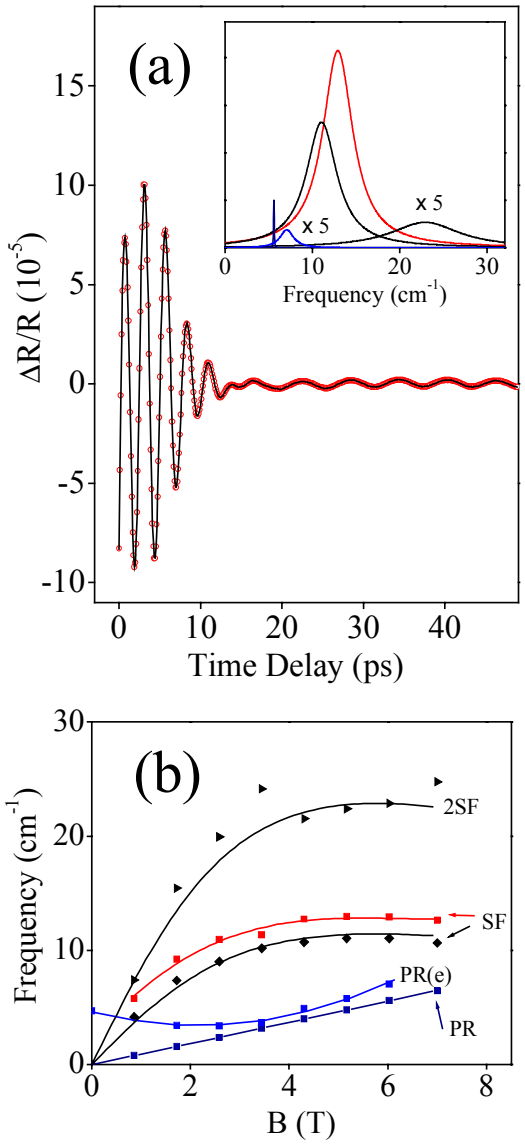

Fig. 7. (a) Resonant differential reflectivity data at B = 6 T, T = 2K, and $\hbar\omega_C$ = 1.682 eV. Curves are LP fits, the inset shows the associated Fourier transform spectra. The dominant feature is the doublet of the electron spin-flip. 1SF shows an overtone at 23 cm^{-1} which reflects coherence involving two electrons (2SF). The sharp feature is the Mn^{2+} paramagnetic resonance. The weak feature at 7 cm^{-1} is assigned to the Mn^{2+} spin-flip in the excited state. (b) Frequency versus magnetic field. 1SF and 2SF curves are fits with x = 0.41% and T=5.5K.

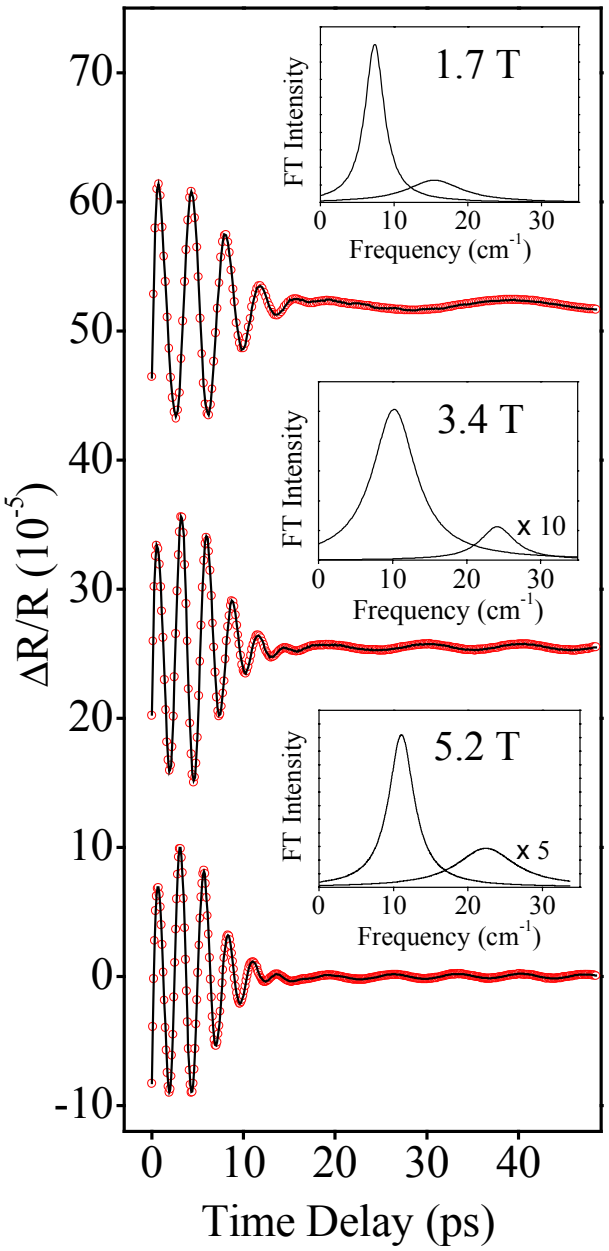

Fig. 8. Differential reflectivity data at three different magnetic fields. The laser energy and temperature are the same as those in Fig. 7. The Fourier transform spectra in the insets show 1SF and 2SF.

assigned as follows. The weak PR line is the ground state coherence of Mn^{2+} ions showing a long dephasing time. The feature labeled PR(e) with slightly higher frequency than PR is attributed to the excited coherence of the Mn^{2+} spin-flip.[9] The curves labeled 1SF represent electron spin-flip transitions. The low frequency 1SF is assigned to the ground state coherence of the donor spin-flip whereas the high frequency 1SF is attributed to electron spin-flip excitations of photo-excited excitons.[9] The feature labeled 2SF, at twice the frequency of 1SF, is assigned to the two-electron ground state coherence. This is supported by the good agreement between pump-probe and Raman scattering experiments since the donor 1SF and 2SF peaks are fitted with the same parameters. This assignment is further supported by the observation that the harmonics are resonant at $\hbar\omega_C = 1.7$ eV. Since an electron has spin $s = \Omega$, the observation of 2SF indicates that we have an entangled state of at least two electrons.

Additional support for the above assignment is as follows. First, the SF line width from pump-probe Fourier transform spectra is comparable to that from spontaneous Raman scattering. We believe that the inhomogeneity of the exciton energy is the major source for the line broadening. Because the frequency of the PR(e) line is also affected by the exciton, the PR(e) oscillation has a width comparable to that of SF. This is in large contrast with the much narrower line width for the PR oscillation in the ground state. Second, the dependence of the excited state frequency agrees very well with our assignment. The Zeeman splitting of the excited state is determined by the total magnetic field, i. e., by both the external magnetic field and the effective field from the heavy hole. At a large external magnetic field, the frequency of the excited state coherence approaches that of the ground state coherence. With a small external magnetic field, the frequency is defined by the effective magnetic field, which is determined by the exchange coupling. The observed PR(e) oscillation frequency agrees quite well with the above argument. The PR(e) approaches 4.7 cm^{-1} which corresponds to an effective magnetic field of 5 T. This value for the effective magnetic field also agrees with a simple estimate based on the known *sp-d* exchange constant and the diameter of the exciton wave function. Based on our model, Raman and pump-probe data, the multiple spin-flip Raman scattering of Mn^{2+} ions and the observation of the single frequency of PR indicates that, in addition to donor entanglement, we have an entangled state involving at least two Mn^{2+} ions.[9]

The frequency difference between the 1SF ground state coherence of donor electrons and the excited state coherence of the electron in the exciton gives also a quantitative estimate of the exchange interaction between the heavy hole and the electron. Using the measured values, we obtain an upper limit of ~ 600 μeV for the electron-heavy-hole exchange interaction which is consistent with the value 270 μeV from the literature.[9,49]

Fig. 9 shows further resonant pump-probe data. Time-domain traces and their Fourier spectra are shown in (a). Only SF and its harmonics are displayed. Fig. 9(b) shows the magnetic field dependence of the SF frequency. Besides the second harmonic, 2SF, the third harmonic, 3SF,

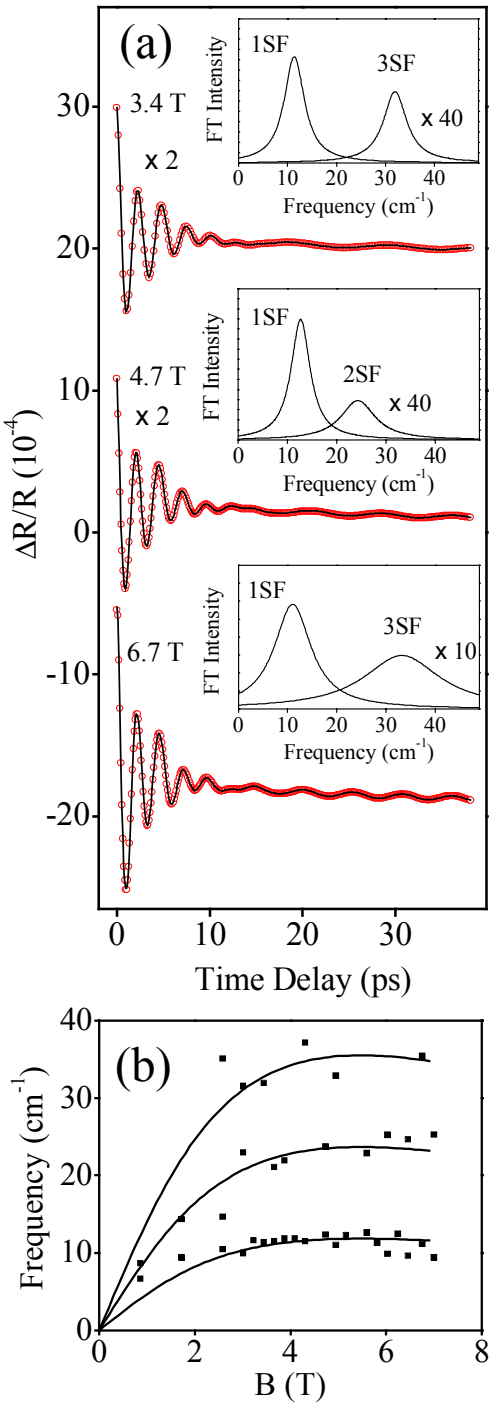

Fig. 9. Resonant pump-probe data at $T = 2$ K and $\hbar\omega_C = 1.687$eV. (a) Differential reflectivity and the associated Fourier transform spectra at three different magnetic fields. The third harmonic electron spin-flip is denoted by 3SF. (b) Magnetic field dependence of the donor spin-flip harmonics. Curves are fits with $x = 0.41\%$ and $T = 5.5$K.

is also observed. Their dependence on magnetic field and temperature agrees well with Raman scattering results. Then, 3SF is assigned to the coherence of three donor electrons, indicating the entanglement of three electrons.

As the laser pulse energy is tuned away from the resonance with localized excitons, the oscillation amplitude for the single electron spin-flip starts to decrease. However, when we tune the laser to resonate with free excitons, relatively strong second and third harmonics are observed. Fig. 10 shows strong second and third harmonic for $\hbar\omega_C$ = 1.71eV. These results clearly indicate that bound-electron entanglement benefits from the mediation of the continuum. However, the process by which the entanglement is attained is not well understood. We note that a mechanism involving the RKKY interaction between localized electrons and delocalized excitons has been previously proposed.[10]

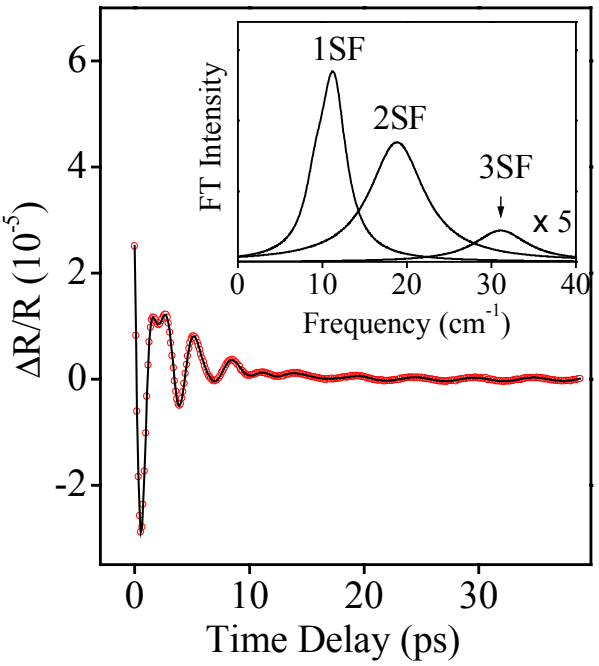

Fig. 10. Differential reflectivity data at B = 7T, T =2K and $\hbar\omega_C$ = 1.71eV (above the gap). The inset is the Fourier transform spectra.

4. CONCLUSIONS

In conclusion, our results confirm that there is a system of localized excitons coupled to paramagnetic impurities in a CdTe quantum well that is well described by the level structure of Fig. 2. We have shown that such a system can be optically excited to generate many-spin Raman coherences and, thus, entanglements involving multiple impurities. Our system of paramagnetic impurities is a promising candidate for meeting the five criteria put forth by DiVincenzo for the physical realization of a quantum computer.[64] Within this context, we note that (*i*) the qubits embodied by the impurity spin states are well characterized and fully scalable, (*ii*) a well-defined initial state can be simply attained by cooling the sample down to sufficiently low temperatures, and (*iii*) spin-flip decoherence times are some of the longest known in the solid phase.[47] We further note that the localization centers associated with, say, surface roughness, and the donors need not be at the same sites. Hence, (*iv*) spectral discrimination coupled with submicrometer-sized apertures[8] can possibly be used to excite particular excitons to address a particular set of impurities. Finally, (*v*) our observations of two- and three-qubit entanglement can be construed as a demonstration of light-controlled interaction between the qubits and, as such, they represent a crucial step for the implementation of a universal set of quantum gates.

5. ACKNOWLEDGMENTS

Work supported by the NSF under Grants No. PHY 0114336 and No. DMR 0072897, by the AFOSR under contract F49620-00-1-0328 through the MURI program and by the DARPA-SpinS program. Acknowledgment is made to the donors of The Petroleum Research Fund, administered by the ACS, for partial support of this research. One of us (AVB) acknowledges partial support from CONICET, Argentina.

REFERENCES

1. J. A. Wheeler and W. H. Zurek, *Quantum Theory and Measurements* (University Press, Princeton, 1983).
2. See: M. A. Nielsen and I. L. Chuang, *Quantum Computation and Quantum Information* (University Press, Cambridge, 2000); and references therein.
3. P. W. Shor, in *Proceedings 35th Annual Symposium on Foundations of Computer Science*, (IEEE Press, Los Alamitos CA, 1994).
4. L. Grover, *Phys. Rev. Lett.* **79**, 325 (1997).

5. P. G. Kwiat, A. J. Berglund, J. B. Altepeter and A. G. White, *Science* **290**, 498 (2000).
6. A. Rauschenbeutel *et al*., *Science* **288**, 2024 (2000).
7. C. A. Sackett *et al*., *Nature* **404**, 256 (2000).
8. G. Chen *et al*., *Science* **289**, 1906 (2000).
9. J. M. Bao, A. V. Bragas, J. K. Furdyna, and R. Merlin, *Nature Mater.* **2**, 175 (2003).
10. C. Piermarocchi, P. Chen, L. J. Sham and D. G. Steel, *Phys. Rev. Lett.* **89**, 167402 (2002); D. P. DiVincenzo *et al.*, *Nature* **408**, 339 (2000).
11. L. M. K. Vandersypen *et al*., *Nature* **414**, 883 (2001).
12. D. Leibfried *et al*., *Nature* **422**, 412 (2003).
13. F. Schmidt-Kaler *et. al*., *Nature* **422**, 408 (2003).
14. G. Burkard, D. Loss and D. P. DiVincenzo, *Phys. Rev. B* **59**, 2070 (1999); J. L. O'Brien, et al. *Phys. Rev. B* **64**, 161401 (2001).
15. X. Li *et al*., *Science* **301**, 809 (2003)
16. J. K. Furdyna*, J. Appl. Phys.* **64**, 29 (1988).
17. J. K. Furdyna and J. Kossut (ed), *Diluted Magnetic Semiconductors, Semiconductors and Semimetals,* Vol. 5 (Academic Press, San Diego CA, 1988).
18. A. K. Ramdas and S. Rodriguez, in *Light Scattering in Solids VI*, Ch. 4, ed. by M. Cardona and G. G¸ ntherodt (Springer, Berlin, 1991).
19. M. Hirsch, R. Meyer and A. Waag, *Phys. Rev. B* **48**, 5217 (1993).
20. J. St¸ hler *et al.*, *Phys. Rev. Lett.* **74**, 2567 (1995); ibid. **74**, 4966 (1995); *J. Crystal Growth* **159**, 1001 (1996).
21. R. W. Martin *et al*., *Phys. Rev. B* **42**, 9237 (1990).
22. C. Benoit ‡ la Guillaume and P. Lavallard, *Phys. Stat. Sol. (b)* **70**, K143 (1975).
23. W. Ungier and M. Suffczynski, *Phys. Rev. B* **27**, 3656 (1983).
24. Y. R. Shen, *The Principles of Nonlinear Optics* (Wiley, New York, 1984).
25. J. Diels and W. Rudolph, *Ultrashort Laser Pulse Phenomena: Fundamentals, Techniques and Applications on a Femtosecond Time Scale* (Academic Press, New York, 1996).
26. Y.-X. Yan, E. Gamble Jr. and K. Nelson, *J. Chem. Phys.* **83**, 5391(1985).
27. R. Merlin*, Solid State Commun.* **102**, 207 (1997).
28. A. T. N. Kumar, F. Rosca, A. Widom and P. M. Champion, *J. Chem. Phys.* **114,** 701 (2001).
29. W. T. Pollard, S. Y. Lee and R. A. Mathies, *J. Chem. Phys.* **92,** 4012 (1990).
30. T. E. Stevens, Ph.D. Thesis, University of Michigan, 2000.
31. T. E. Stevens, J. Kuhl and R. Merlin, *Phys. Rev. B* **65,** 144304 (2002).
32. Mechanisms for multiple spin-flip RS are closely related to those for overtones of longitudinal-optical phonons; see, *e.g.*, R. Merlin, *et al.*, *Phys. Rev. B* **17**, 4951 (1978).
33. P. Y. Yu and M. Cardona, *Fundamentals of Semiconductors* (Springer, Berlin, 2001).
34. W. S. Warren, H. Rabitz and M. Dahleh, *Science* **259**, 1581 (1993).
35. I. R. Sola, J. Santamaria and D. J. Tannor, *J. Phys. Chem. A* **102**, 4301 (1998).
36. S. Shi and H. Rabitz, *J. Chem. Phys*. **92**, 2927 (1990).
37. K. V. Kavokin and I. A. Merkulov, *Phys. Rev. B* **55**, R7371 (1997).
38. K. Bergmann and B. W. Shore, in *Molecular Dynamics and Spectroscopy by Stimulated Emission Pumping*, ed. by H. L. Dai and R. W. Field (World Scientific, Singapore, 1995).
39. A. A. Sirenko *et al.*, *Phys. Rev. B* **56** (1997) 2114.
40. E. N. Economou, J. Ruvalds and K.L. Ngai, *Phys. Rev. Lett.* **29,** 110 (1972).
41. J. F. Scott, T. C. Damen and P. A. Fleury, *Phys. Rev B* **6,** 3856 (1972).
42. J. F. Scott and T. C. Damen, *Phys. Rev. Lett.* **29**, 107 (1972).
43. P. Hiesinger, S. Suga, F. Willmann and W. Dreybrodt, *Phys. Stat. Sol. (b)* **67**, 641 (1975).
44. S. Suga, *et al.*, *Solid State Commun.* **15**, 871 (1974).
45. W. Ungier, M. Suffczynski and J. Adamowski, *Phys. Rev. B* **24**, 2109 (1981).
46. S. A. Crooker, D. D. Awschalom and N. Samarth, *IEEE J. Sel. Top. Quantum Electron.* **1**, 1082 (1995).
47. S. A. Crooker *et al.*, *Phys. Rev. B* **56**, 7574 (1997).
48. H. Barkhuijsen *et al.*, J. Mag. Res. **61**, 465 (1985); F. W. Wise, M. J. Rosker, G. L. Millhauser and C. L. Tang, *IEEE J. Quantum Electron.* **QE-23**, 1116 (1987).
49. L. Besombes, K. Kheng and D. Martrou, *Phys. Rev. Lett.* **85,** 425 (2000).
50. S. A. Wolf *et al.*, *Science* **294**, 1488 (2001).

51. M. Z. Maialle, E. A. De Andrada e Silva, and L. J. Sham, *Phys. Rev. B* **47**, 15776 (1993).
52. S. Bar-Ad and I. Bar-Joseph, *Phys. Rev. Lett.* **66**, 2491 (1991).
53. A. S. Lenihan *et al*., *Phys. Rev. Lett.* **88**, 223601 (2002).
54. K. B. Ferrio and D. G. Steel, *Phys. Rev. Lett.* **80**, 786 (1998).
55. B. E. Larson, K. C. Hass and R. L. Aggarwal, *Phys. Rev. B* **33,** 1789 (1986).
56. D. U. Bartholomew *et al*., *Solid State Commun.* **62**, 235 (1987).
57. R. Rupprecht *et al.*, Phys. Rev. B. **63**, 115325 (2001).
58. M. Trigo *et al*., *Phys. Rev. Lett.* **89**, 227402 (2002).
59. C.-K. Sun, J.-C. Liang, and X.-Y. Yu, *Phys. Rev. Lett.* **84**, 179 (1999).
60. G. C. Cho, W. K¸ tt and H. Kurz, *Phys. Rev. Lett.* **65**, 764 (1990).
61. R. W. G. Syme, D. J. Lockwood, M. M. Dion and J. J. Dubowski, *Solid State Commun*. **103**, 239 (1997).
62. J. M. Rowe, R. M. Nicklow, D. L. Price and K. Zanio, *Phys. Rev. B* **10**, 671 (1974).
63. M. H. Krisch *et al.*, *Phys. Rev. Lett.* **56**, 8691 (1997).
64. D. P. DiVincenzo, *Fortschr. Physik* **48**, 771 (2000).